Journal of Ceramic Processing Research. Vol. 17, No. 4, pp. 356~359 (2016)

J O U R N A L O F
Ceramic Processing Research

Structural properties of $limn_2o_4$ thin films deposited by rf magnetron sputtering

Ji Hwan Bae[a], Dong Hyun Hwang[b], Shin Ho Cho[b], Jung Dae Kim[b] and Young Guk Son[a,*]

[a]*Department of Materials Science and Engineering, Pusan National University, Busan, 609-735, Korea*
[b]*Department of Materials Science and Engineering, Silla University, Busan, 617-736, Korea*

Lithium manganese oxide ($LiMn_2O_4$) cathode thin films were deposited on a Si substrate by radio frequency (RF) magnetron sputtering. The films were annealed within the range 400 to 700 °C for 2 h in O_2. Structure and surface morphology of the films were characterized by X-ray diffraction (XRD) and field emission scanning electron microscopy (FESEM). Elemental analysis was conducted by energy dispersive spectroscopy (EDS). The degree of crystallization in the films increases with annealing temperature. A phase transformation from the amorphous to the crystalline phase is apparent at around 600 °C. Films annealed at 700 °C exhibit characteristic XRD peaks with a predominant (111) orientation representing cubic spinel structure. The lattice parameter is 6.694 Å for the 700 °C annealed film. The grain size gradually increases with annealing temperature, as evident from the SEM images.

Key words: $LiMn_2O_4$ thin film, Lithium battery, RF magnetron sputtering.

Introduction

Recent increasing demands for portable electrical devices have created a need for smaller batteries. For this application, the rechargeable lithium film battery has attracted much attention. Many rechargeable batteries have been studied in the search for high energy density, reduced memory effect, long cycle life, and high output power. Lithium film batteries are found in various commercial applications, such as pocket-sized medical devices and mobile phones.

Presently, the most widely used cathode material in lithium ion thin film batteries is $LiCoO_2$. However, $LiCoO_2$ has disadvantages such as high cost, a limited source of cobalt material, and safety concerns, which limit its application [1]. A promising alternative is spinel $LiMn_2O_4$, based on MnO. Spinel $LiMn_2O_4$ has the characteristics of relatively low cost, environmental friendliness, and excellent structural stability [2]. However, $LiMn_2O_4$ has problems due to Mn dissolution at elevated temperature in electrolyte ($2Mn^{+3} \rightarrow Mn^{+4} + Mn^{+2}$) [3], occurrence of Jahn-Teller distortion [4], and crystallinity loss during cycling [5]. The deterioration of cycling characteristics caused by Jahn-Teller distortion is a well-known result of the phase transition into tetragonal form, caused by an increased c/a axial ratio during lithium insertion in the 3 V charge-discharge region [6].

There are several methods available to fabricate $LiMn_2O_4$ thin film cathode materials, including electron beam evaporation [7, 8], electrostatic spray deposition [9], and RF magnetron sputtering. Among these, the most versatile is the RF magnetron sputtering technique, owing to its ability to deposit a thin film on flexible substrates, with a lower probability of the film separating from the substrate than with other techniques. Wu et al. [10] investigated the effect of thickness on the properties of solution-deposited $LiMn_2O_4$ thin films at 750 °C. Moon *et al*. [11] studied electrochemical properties of $LiMn_2O_4$ thin films at 750 °C. Babu *et al*. [12] presented structure and electrochemical properties for deposition at various substrate temperatures. In general, post-annealing can drive the rearrangement of atoms and eliminate defects, increasing the quality of grown thin films.

In this paper, $LiMn_2O_4$ thin films were sought with the optimal spinel structure for application in miniaturized electronic devices. $LiMn_2O_4$ thin films were deposited on silicon wafers using RF magnetron sputtering at room temperature, post-annealed, and subsequently, their structural and surface properties were studied.

Experimental

$LiMn_2O_4$ thin films were deposited on silicon wafer substrates using RF magnetron sputtering (13.56 MHz). The Si wafers were cleaned in an ultrasonic bath sequentially with ethanol, acetone and DI water, and moisture was removed with N_2 gas. The target used was commercially available 2-inch diameter $LiMn_2O_4$ (purity 99.99%); the distance between substrate and target was approximately 5 cm. A base vacuum of 6×10^{-5} Torr was obtained using process gas. Before deposition, the $LiMn_2O_4$ target was cleaned by pre-sputtering in an argon atmosphere for 10 min to

*Corresponding author:
Tel : +82-51-510-2445
E-mail: ykson@pusan.ac.kr

Table 1. Deposition conditions for $LiMn_2O_4$ thin films.

Parameter	Condition
Target	$LiMn_2O_4$ (99.99% pure)
Substrate	Silicon wafer, p-type (111)
RF power	120 W
Sputtering pressure	3×10^{-2} Torr
Substrate temperatures	Room temperature
Target to substrate distance	50 mm

eliminate surface oxide layers. During sputtering, RF power is maintained at 120 W and the working pressure is kept at 3×10^{-2} Torr. The sputtered films were annealed in an oxygen atmosphere at temperatures between 400 and 700 °C. The deposition conditions are summarized in Table 1.

Crystalline structure of the thin films was characterized by X-ray diffraction (XRD), using Cu-Kα radiation (Ultima IV). Surface morphology of the $LiMn_2O_4$ thin films was characterized by field-emission scanning electron microscopy (FE-SEM), (MIRA III). The composition of films deposited on silicon substrates was observed by energy dispersive spectroscopy (EDS) and analyzed using energy dispersive X-ray analysis (EDAX).

Results and Discussion

All deposited samples were a dark red color under visible light. Fig. 1 shows an SEM cross-sectional photograph of $LiMn_2O_4$ thin film on the silicon substrate. The average film thickness is found to be about 0.2 μm, and the deposition rate calculated to be 2.8 nm/min.

Fig. 2 shows the X-ray diffraction patterns of $LiMn_2O_4$ thin films post-annealed at various temperatures in air for 2 h. The silicon substrate peak appears at around $2\theta = 59°$. For thin films that are as-deposited and annealed at 400 °C, only the substrate peak appears clearly, indicating that the crystallinity is very low, with a possible peak occurring at

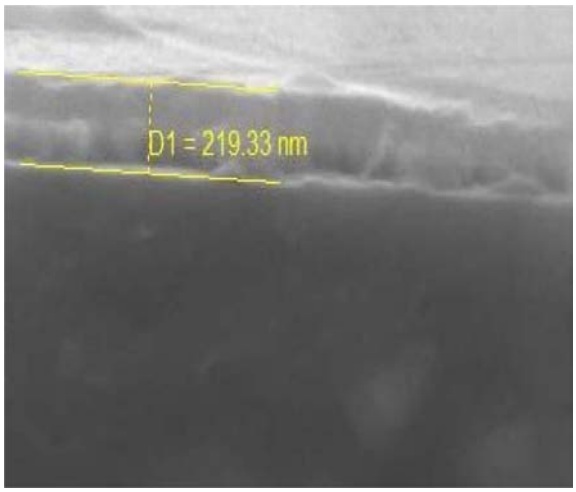

Fig. 1. SEM cross-sectional image of a $LiMn_2O_4$ thin film on Si wafer, as-deposited by RF magnetron sputtering.

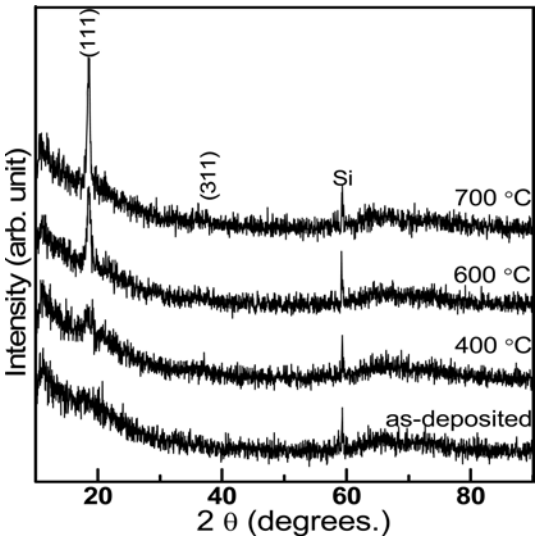

Fig. 2. XRD patterns of the $LiMn_2O_4$ thin films deposited on Si substrate, annealed at various temperatures.

around $2\theta = 20.2°$ [13]. This implies that, owing to the low annealing temperature, very little crystallinity is formed. With an increase in the annealing temperature, the peak becomes more intense and sharper. For the sample annealed at 600 °C, a main peak and a weaker peak are seen: the main peak occurs at $2\theta = 18.56°$, which corresponds to reflection from the $LiMn_2O_4$ (111) plane. The weaker peak occurs at around $2\theta = 36°$, corresponding to the (311) plane of $LiMn_2O_4$. It can be clearly seen that the transformation from an amorphous to a crystalline phase occurs at around 600 °C. When the annealing temperature is increased to 700 °C, there appears to be a close match to a cubic spinel structure of Fd3m symmetry, in which Li-ions occupy the 8a tetrahedral sites and manganese cations occupy the 16d octahedral sites of a cubic close-packed array constituted by oxygen located in the 32e positions. At 700 °C, the full width at half-maximum (FWHM) of the (111) peak is found to be about 0.54°. The average grain size in the $LiMn_2O_4$ thin film annealed at 700 °C is 15 nm, as calculated by the Scherrer formula [14]:

$$D = 0.9\,\lambda / (\beta \cdot \cos\theta), \quad (1)$$

where l is the X-ray wavelength (0.15406 nm), β is the angular line width at half-maximum intensity of the peak at 2θ, and θ is the Bragg diffraction angle.

The XRD patterns show that with increased annealing temperatures, there is a slight shift in peak positions toward lower diffraction angles. This shift in peak positions may be due to strain in the film, arising from ion bombardment during sputter deposition [15]. The results are in good agreement with those reported by Tomy *et al* [16]. However, Son [17] reported the opposite result, with peak positions shifted toward higher angles with increased annealing temperature. These XRD results on $LiMn_2O_4$ films demonstrate that

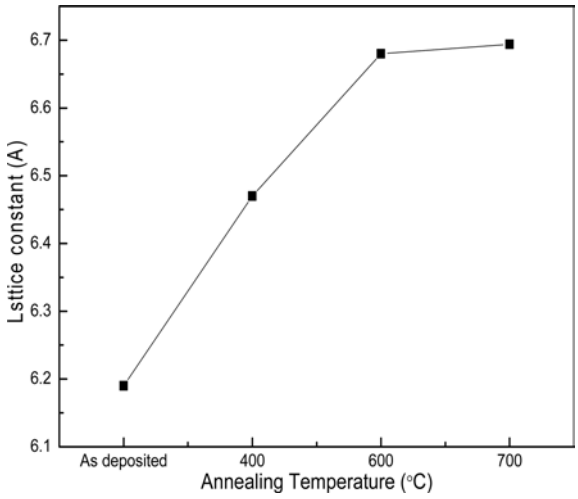

Fig. 3. The lattice constant of $LiMn_2O_4$ thin film as a function of post-annealing temperature.

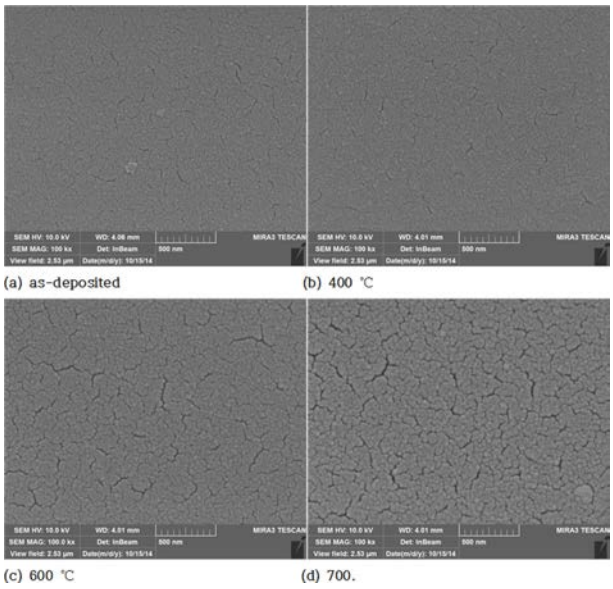

Fig. 4. SEM images of $LiMn_2O_4$ thin films, as-deposited, and post-annealed at various temperatures for 2 h in O_2.

crystallinity of the films significantly improves with increased post-annealing temperature.

The lattice parameters of $LiMn_2O_4$ thin films deposited on silicon substrates and post-annealed at various temperatures are shown in Fig. 3. The lattice constants are calculated from the predominant (111) peaks. For as-deposited film, the lattice constant is found to be about 6.190 Å; it gradually increases with increased annealing temperature. The greatest lattice parameter observed, 6.694 Å, is for the film annealed at the highest temperature, 700 °C. This value is about 1.5 Å less than that reported by Tomy *et al* [16]. The expected value for the $LiMn_2O_4$ spinel structure is 8.24 Å; however, our observed lattice parameter is smaller because of compressional stresses in the films. Higher annealing temperatures provide the kinetic energy for rearrangement within grown thin films with elevated grain sizes. This is evident from the XRD result as well. As particle size increases, the volume of the deposited film expands and the lattice increases. Moreover, the higher surface thermal energy changes the valence state of transition elements. These reasons account for the increased lattice parameter [12].

Surface morphology of the $LiMn_2O_4$ thin films was studied by FE-SEM measurements. Fig. 4 shows SEM images of the post-annealed $LiMn_2O_4$ thin films for various annealing temperatures. The as-deposited film and the film annealed at 400 °C do not show clear surface structure, and the amorphous nature seen in the images indicates a low degree of crystallinity. With increasing annealing temperature, the morphological changes show a noticeable increase in grain size. The film annealed at 700 °C shows more growth and more regular particles compared to the films that are as-deposited and annealed at 400 °C; the particles are found to have an average diameter of around 50 nm for 700 °C annealing temperature. We observe that the grain sizes are increased with increased annealing temperature, as nucleation is promoted at lower temperature and suppressed at higher. As a result, when nucleation is suppressed, crystal growth is promoted. Also, as the annealing temperature increases, the lattice of the deposited films expands and the volume increases,

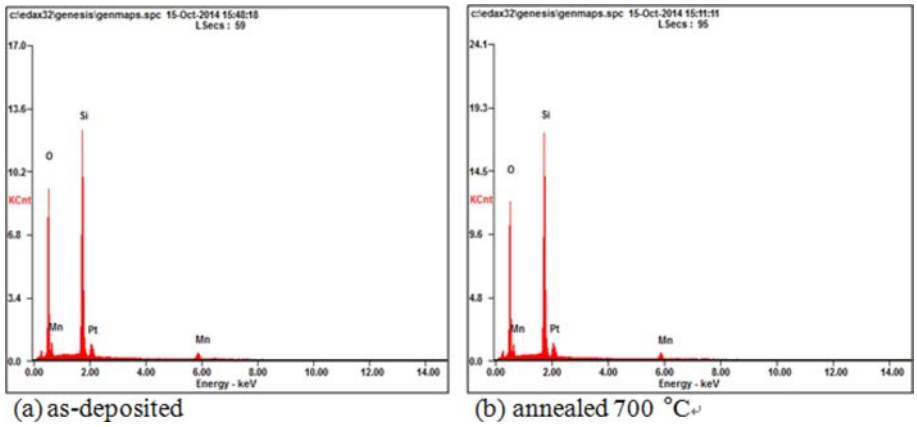

Fig. 5. EDS images of $LiMn_2O_4$ thin films, as-deposited, and annealed at 700 °C.

owing to strain in the film [15].

As-deposited and annealed (700 ºC) EDS measurements are shown in Fig. 5. The peak detected at about 1.5 KeV in both Fig. 5(a) and (b) is the Si substrate peak. Two elements (O, Pt) each have one line between 0 and 8KeV, and the other element (Mn) has two lines at about 0.5 and 6 KeV. The Pt element observed is because of a thin-film surface coating deposited for the SEM and EDS measurements. One overlap is observed for O and Mn in the low energy region. Lithium cannot be observed in Fig. 5 as Li atoms have small atomic number. With increased annealing temperature, no new elements appear in the EDS trace, however the intensity of oxygen is observed to be weaker.

Conclusions

The effects of post-annealing temperature on the structural and surface morphological properties of $LiMn_2O_4$ thin films deposited on a silicon wafer substrate by RF magnetron sputtering were investigated. The films show a predominant (111) orientation representing cubic spinel structure with Fd3m symmetry. Transformation from the amorphous to crystalline phase is clearly found at around 600 ºC. The largest grain size observed via XRD linewidth is 15 nm at 700 ºC. The lattice parameter increases from 6.190 to 6.694 Å with increased annealing temperature. The particle size was observed in SEM images to be larger with increased annealing temperature. The elements (Si, O, Mn, Pt) are observed by EDS measurement. It can be concluded that the post-annealing of $LiMn_2O_4$ thin films can significantly improve their structural and surface morphological properties.

Acknowledgments

This work was supported by a 2-Year Research Grant of Pusan National University.

References

1. J. Fischer, C. Adelhelm, T. Bergfeldt, K. Chang, C. Ziebert, H. Leiste, M. Stuber, S. Ulrich, D. Music, B. Hallstedt and H. J. Seifert, Thin Solid Films. 528 (2013) 217-223.
2. J.M. Tarascon and D. Guyomard, Electrochim. Acta. 38 (1993) 1221.
3. R.J. Gummow, A. de Kock and M.M. Thackeray, Solid State Ionics. 69 (1994) 59.
4. M.M. Thackeray, Y. Shao-Horn, A.J. Kahaian, K.D. Kepler, E. Skinner, J. T. Vaughey and S.J. Hackney, Electrochem. Solid-State Lett. 1 (1998).
5. H. Huang, C.A. Vincent and P.G. Bruce, J. Electrochem. Soc. 146 (1999) 3649.
6. B.S. Kim and Y.G. Son, J. Research Inst. Ind. Technol. 58 (2000) 43-50
7. F.K. Shokoohi, J.M. Tarascon and B.J. Wilkens, J. Appl. Phys. Lett. 59 (1991) 1260.
8. F.K. Shokoohi, J.M. Tarascon, B.J. Wilkens, D. Guyomard and C.C. Chang, J. Electrochem. Soc. 139 (1992) 1845.
9. D. Shu, K. Y. Chung, W.I. Cho and K.B. Kim, J. Power Sources. 114 (2003) 253.
10. Xian Ming Wu, Ze Qiang He, Shang Chen, Ming You Ma, Zhuo Bing Xiao and Jian Ben Liu, Mater. Chem. Phys. 105 (2007) 58-61.
11. H.S. Moon, W.H. Lee, Philip J. Reucroft and J. W. Park, J. Power Sources. 119-121 (2003) 710-712.
12. K. Jayanth Babu, P. Jeevan Kumar and O. M. Hussain, Appl Nanosci. 2 (2012) 401-407.
13. S. Komaba, N. Kumagai, M. Baba, F. Miura, N. Fujita, H. Groult, D. Devilliers and B. Kaplan, J. Appl. Electrochem. 30 (2000) 1179-1182.
14. B. D. Cullity and S. R. Stock, Elements of X-ray Diffraction, (third ed), Prentice-Hall Inc (2001).
15. S. Surampudi, Electrochem. Soc. Proc. 280 (1999) 98-16.
16. M. R. Tomy, K. M. Anil Kumar, P. B. Anand and S. Jayalekshmi, J.Phys. Chem. Solids. 72 (2011) 1251-1255.
17. Y.G. Son, J, Research Inst. Ind. Technol. 52 (1997) 123-134.